Two-Dimensional NMR Studies of the Zinc Finger Motif: Solution Structures and Dynamics of Mutant ZFY Domains Containing Aromatic Substitutions in the Hydrophobic Core[†,‡]

Xiuqi Qian[§] and Michael A. Weiss[*,§,‖]

Department of Biological Chemistry and Molecular Pharmacology, Harvard Medical School, Boston, Massachusetts 02115, and Department of Medicine, Massachusetts General Hospital, Boston, Massachusetts 02114

Received January 28, 1992; Revised Manuscript Received May 18, 1992

ABSTRACT: Solution structures of mutant Zn fingers containing aromatic substitutions in the hydrophobic core are determined by 2D-NMR spectroscopy and distance-geometry/simulated annealing (DG/SA). The wild-type domain (designated ZFY-6) is derived from the human male-associated protein ZFY and represents a sequence motif (Cys-X_2-Cys-X-Ar-X_7-Leu-X_2-His-X_4-His) that differs from the consensus (Cys-$X_{2,4}$-Cys-X_3-Phe-X_5-Leu-X_2-His-X_3-His) in the location ("aromatic swap") and diversity (Ar = tyrosine, phenylalanine, or histidine) of the central aromatic residue (underlined). In a given ZFY domain the choice of a particular aromatic residue is invariant among vertebrates, suggesting that alternative "swapped" aromatic residues are functionally inequivalent. 2D-NMR studies of analogues containing tyrosine, phenylalanine, or histidine at the swapped site yield the following results. (i) The three DG/SA structures each retain the $\beta\beta\alpha$ motif and exhibit similar staggered-horizontal packing between the variant aromatic residue and the proximal histidine in the hydrophobic core. (ii) The structures and stabilities of the tyrosine and phenylalanine analogues are essentially identical, differing only by local exposure of polar (Tyr *p*-OH) or nonpolar (Phe *p*-H) surfaces. (iii) The dynamic stability of the histidine analogue is reduced as indicated by more rapid protein–deuterium exchange of hydrogen bonds related to secondary structure and amide–sulfur coordination (slowly exchanging amide resonances in D_2O) and by more extensive averaging of main-chain dihedral angles ($^3J_{\alpha NH}$ coupling constants). An aspartic acid in the putative DNA recognition surface, whose configuration is well-defined as a possible helix N-cap in the tyrosine and phenylalanine analogues, exhibits multiple weak main-chain contacts in the NOESY spectrum of the histidine analogue; such NOEs are geometrically inconsistent and so provide complementary evidence for structural fluctuations. (iv) Because the three DG ensembles have similar apparent precision, the finding of reduced dynamic stability in the histidine analogue emphasizes the importance of experiments that directly probe fluctuations at several time scales. Our results provide insight into the design of biological metal-binding sites and the relationship of protein sequence to structure and dynamics.

The classical Zn finger motif (X_3-Cys-X_2-Cys-X_3-Phe-X_5-Leu-X_2-His-X_4-His-X_4) defines a highly conserved class of eukaryotic nucleic acid binding proteins involved in the regulation of gene expression (Klug & Rhodes, 1987). Single Zn fingers exhibit metal-dependent folding (Frankel et al., 1987) as globular minidomains (Parraga et al., 1988). 2D-NMR[1] structures of isolated domains (Lee et al., 1989a,b; Klevit et al., 1990; Omichinski et al., 1990) are essentially identical to those of corresponding domains in the crystal structure of a protein–DNA complex containing three fingers (Pavletich & Pabo, 1991). The isolated Zn finger thus provides a model for investigation of folding rules in a simple sequence template (the $\beta\beta\alpha$ motif; Berg, 1988; Gibson et al., 1988). Insight into the informational content of this template (Bowie et al., 1990) may be obtained by analysis of patterns of conservation and divergence among Zn finger sequences.

In previous studies we have investigated the implications of sequence variations among Zn finger domains for thermodynamic stability[2] (Weiss et al., 1990; Weiss & Keutmann, 1990) and structure (Kochoyan et al., 1991a–d; Jasanoff et al., 1992). These investigations have focused on the ZFY-related family of putative transcription factors (Page et al., 1987). This family is encoded by the sex chromosomes of placental mammals (Schneider-Gadicke et al., 1989); homologues are also observed among marsupial mammals, birds, and reptiles (DiLella et al., 1990). ZFY is the prototype of a class of variant Zn finger proteins defined by an alternating pattern of finger and linker sequences (Page et al., 1987; Nietfeld et al., 1989; Weiss et al., 1990). Whereas odd-numbered ZFY domains follow the classical Zn finger consensus, even-numbered domains follow the pattern X_3-Cys-X_2-Cys-X-Ar-X_7-Leu-X_2-His-X_4-His-X_4, which differs in the placement ("swap") of the central aromatic residue (Ar) and in the spacing between histidines (His-X_4-His). The solution structure of a representative even domain (ZFY-6) retains the $\beta\beta\alpha$

† Supported by grants from the National Institutes of Health and the American Cancer Society to M.A.W.

‡ The coordinates of the NMR structures and tables of NMR-based restraints have been deposited in the Brookhaven Protein Data Bank.

* Address correspondence to this author at the Department of Biological Chemistry and Molecular Pharmacology, Harvard Medical School.

§ Harvard Medical School.

‖ Massachusetts General Hospital.

[1] Abbreviations: CD, circular dichroism; DG, distance geometry; DQF-COSY, double-quantum-filtered correlated spectroscopy; NMR, nuclear magnetic resonance; NOE, nuclear Overhauser enhancement; NOESY, NOE spectroscopy; rms, root mean square; ROESY, rotating frame Overhauser spectroscopy; rp-HPLC, reverse-phase high-performance liquid chromatography; SA, simulated annealing; SD, standard deviation; UV, ultraviolet.

[2] In this paper the term *stability* is used in two senses. *Thermodynamic stability* refers to a free-energy difference between the folded and unfolded states; *dynamic stability* refers to structural fluctuations within the folded state.

0006-2960/92/0431-7463$03.00/0

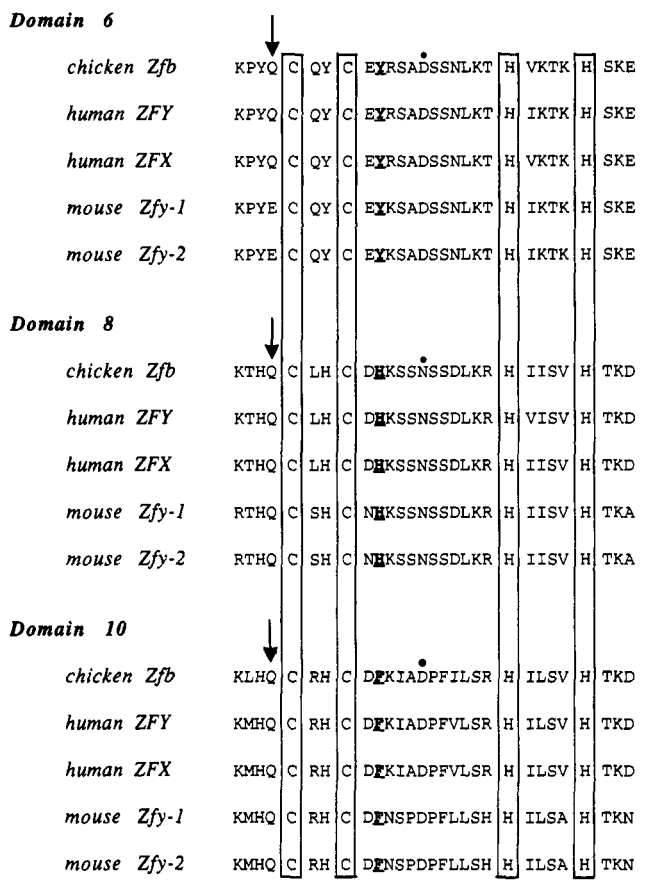

FIGURE 1: Sequences of even-numbered ZFY domains (fingers 6, 8, and 10) demonstrating variation in the identity of the central aromatic residue (F, Y, or H; underlined and boldface) but invariance among vertebrate species within individual domains. Conserved cysteines and histidines, presumed to coordinate Zn^{2+}, are boxed. Arrows indicate conserved glutamine in the β-sheet (Gln4 in the peptide numbering scheme), and dots indicate proposed N-cap aspartic acid or asparagine (Asp14 or Asn14 in the peptide numbering scheme). Previous pH unfolding studies have demonstrated that the stability of human domain 8 is significantly less than that of domain 6 or 10 (Weiss et al., 1990). Sequences are obtained from DiLella et al. (1990).

structure (Kochoyan et al., 1991a,b). 2D-NMR studies of chimeric (even–odd) analogues of ZFY-6 demonstrate, however, that distinguishing features of even sequences are associated with alternative internal architectures and surface topologies (Kochoyan et al., 1991c,d). Implications of such structural variation for mechanisms of DNA binding are not understood and are of interest in relation to nonstandard models of Zn finger–DNA recognition (Fairall et al., 1986; Churchill et al., 1990; Berg, 1990; Kochoyan et al., 1991a; Klevit, 1991).

The present study is motivated by a striking difference between the evolutionary history of odd- (consensus) and even-numbered (nonconsensus) ZFY domains. Among odd ZFY domains (and in the majority of other consensus Zn finger sequences; Gibson et al., 1988) the central aromatic residue is invariant as phenylalanine (X_3-Cys-X_2-Cys-X_3-Phe-X_5-Leu-X_2-His-X_3-His-X_4). Such invariance may have a simple chemical basis: the Phe side chain participates in an internal aromatic–aromatic interaction ("edge to face"; Burley & Petsko, 1985, 1988) in which the para proton packs against the center of the proximal histidine ring (Kochoyan et al., 1991c; Mortishire-Smith et al., 1992). In contrast to the invariance of the consensus phenylalanine, the "swapped" aromatic residue (Ar) among even-numbered ZFY domains may be phenylalanine, tyrosine, or histidine (Figure 1; DiLella et al., 1990). In a particular domain a given aromatic residue is invariant (e.g., Tyr in domain 6 in man, mouse, and bird; Figure 1). What structural similarities underlie the relaxed sequence requirement at the swapped site, and what structural differences account for invariance among individual domains? To address these questions, we have determined the 2D-NMR structures of representative Zn finger peptides containing phenylalanine, tyrosine, and histidine at the swapped position. The overall $\beta\beta\alpha$ motif is retained in each case. These analogues nevertheless exhibit local and nonlocal differences whose comparative analysis provides insight into the design of biological metal-binding sites.

MATERIALS AND METHODS

Peptide Synthesis. The synthesis and characterization of ZFY-6 (KTYQCQYCEYRSADSSNLKTHIKTKHSKEK; Figure 2A) have previously been described (Kochoyan et al., 1991a). This peptide is derived from finger 6 of the putative DNA-binding exon of the human ZFY gene (exon residues 162–191; Page et al., 1987). Analogues ZFY-*phe* (substitution Tyr10Phe; underlined above) and ZFY-*his* (substitution Tyr10His) were synthesized by the solid-phase procedure (Barany & Merrifield, 1979; Steward & Young, 1984) using F-moc methodology (Chang & Meienhofer, 1978; Atherton et al., 1978); the initial residue was linked to a *p*-alkoxybenzyl alcohol resin to provide a C-terminal carboxylic acid. Peptides were reduced and purified by rp-HPLC as described (Weiss et al., 1990; Kochoyan et al., 1991a). The reduced peptide–Zn^{2+} complexes were lyophilized and stored in an anaerobic N_2 chamber (Coy Laboratories, Inc.).

Circular Dichroism. CD spectra were obtained with an Aviv spectropolarimeter at a peptide concentration of 90 μM in a 1-mm path-length cuvette as described (Weiss et al., 1990). CD spectra were obtained in 50 mM Tris-HCl buffer containing 0.1 mM $ZnCl_2$; to obtain unfolding curves, the buffer pH was adjusted in the range 1–9 with 1% acetic acid. Buffers were deoxygenated with N_2 prior to dissolution of peptide.

NMR. ZFY-*phe* (12 mg) and ZFY-*his* (14 mg) were dissolved in 0.7 mL of NMR buffer containing 50 mM deuterated Tris-HCl (pH or pD 6.0; direct meter reading) and 5 mM $ZnCl_2$. Two-dimensional experiments were obtained in 99.98% D_2O and 90% H_2O/10% D_2O at 500 MHz and 25 °C. Double-quantum-filtered correlation spectroscopy (DQF-COSY), total correlation spectroscopy (TOCSY; mixing times 30 and 55 ms), nuclear Overhauser enhancement spectroscopy (NOESY; mixing times 100 and 200 ms), and rotating-frame Overhauser enhancement spectroscopy (ROESY; mixing time 50 ms) experiments were performed by the pure-phase method (States et al., 1982). The data were processed with a combination of exponential and shifted sine-bell window functions in both dimensions. The sweep width was 7000 Hz in each dimension; 350 t_1 increments were obtained. The observed 350 × 4K complex data matrices were zero-filled to 4K × 4K (NOESY, ROESY, and TOCSY) or 4K × 8K (DQF-COSY). $^3J_{\alpha N}$ coupling constants were measured on the basis of the structure of "fingerprint" cross peaks in the DQF-COSY spectrum in H_2O; distortions in apparent multiplet separation arising from finite line widths were corrected by spectral simulation as described (Redfield & Dobson, 1990; Smith et al., 1991). Chemical shifts are measured in parts per million (ppm) relative to H_2O (4.78 ppm at 25 °C).

NMR-Derived Restraints. NOE and *J*-coupling (dihedral angle) restraints were used for molecular modeling as

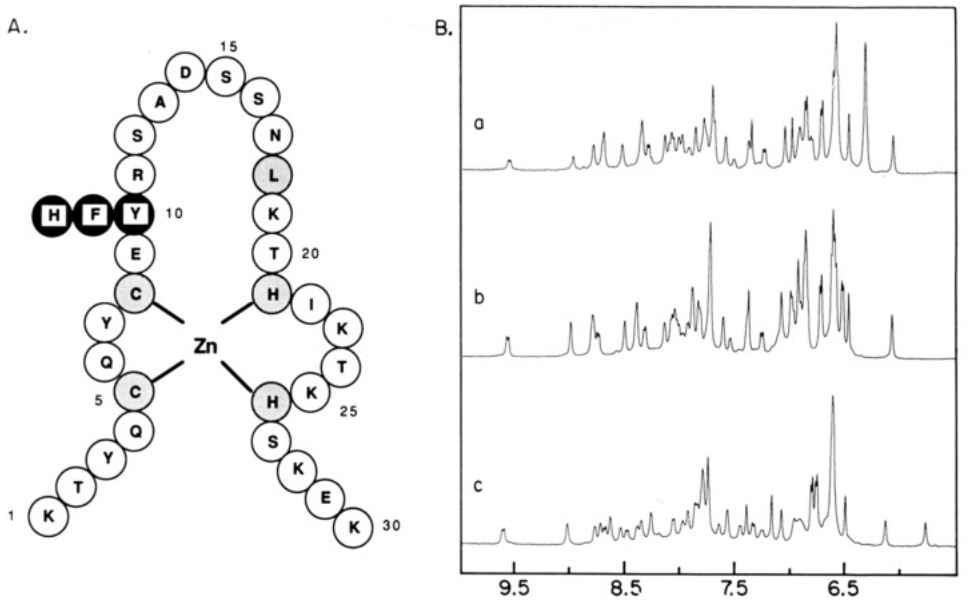

FIGURE 2: (A) Schematic representation of the sequence of ZFY-6. Positions of mutations Tyr10Phe and Tyr10His are indicated by outer circles (heavily shaded); cysteines and histidines presumed to coordinate Zn^{2+} and conserved framework leucine are indicated (lightly shaded). (B) Amide–aromatic region of the ^{1}H-NMR spectra of ZFY analogues in H_2O: (a) ZFY-6 (Kochoyan et al., 1991a), (b) ZFY-*phe*, and (c) ZFY-*his*.

previously described (Kochoyan et al., 1991a,b). NOEs were classified as strong (<2.7 Å), medium (<3.4 Å), or weak (<4.3 Å) on the basis of the amplitude of the NOESY cross peaks relative to the intraresidue ortho–meta cross peak of tyrosine (2.5 Å) and the H_δ–H_ϵ cross peak of histidine (4.3 Å). Distance-bound corrections were made for the methyl groups and methylene protons for which stereospecific assignments could not be obtained (Wuthrich, 1986). Dihedral angle restraints were introduced on the basis of *J*-coupling constants. ϕ dihedral angles of residues with small coupling constants ($^3J_{\alpha NH}$ < 6.0 Hz) were constrained between –100° and –20°; those with large coupling constants ($^3J_{\alpha NH}$ >8.0 Hz) were constrained between –160° and –80°; restraints were not introduced for intermediate *J* values. χ_1 dihedral angles, when obtained (Tables I and II), were restrained about the preferred rotamer with a tolerance of ±40°. Experimental restraints for each analogue are provided as supplementary material. Distance-geometry/simulated annealing (DG/SA) calculations were performed with the program DGII (T. F. Havel, Harvard Medical School).

Hydrogen Bonds. Possible hydrogen bonds in DG structures were calculated with the analysis facility of the program XPLOR (A. T. Brunger, Yale University). Since the simulating annealing protocol of DGII does not contain electrostatic terms or an explicit hydrogen bond potential, potential hydrogen bonds reflect the geometric content of the restraints. We consider as established those hydrogen bonds that are both consistently predicted by the DG models and correspond to slowly exchanging amide resonances in D_2O (asterisks in Tables VI and VII). Possible hydrogen bonds are otherwise considered as stereochemically permitted but not established. In selected cases circumstantial evidence for such additional hydrogen bonds is provided by qualitative features of the NMR data (e.g., the inequivalent H_δ methylene resonances and side-chain NOEs of Gln4; Figure 8); we consider such hydrogen bonds as "proposed" but not established. To accommodate possible hydrogen bonds, distance-geometry calculations were performed in three steps. (i) In the initial calculations distances between atoms were constrained to be greater than the sum of their respectively hard-sphere radii. This default lower bound in principle introduces a systematic error in the distance between hydrogen bond donors and acceptors. (ii) In intermediate calculations the lower bound between presumed amide–carbonyl hydrogen bonds *corresponding to slowly exchanging amide resonances* was reduced from 2.3 to 1.9 Å (H_N···O═C); the lower bound between presumed amide–sulfur hydrogen bonds *corresponding to slowly exchanging amide resonances* was reduced from 2.6 to 2.2 Å (H_N···S—Zn); lower bounds between possible side-chain hydrogen bonds involving Gln4 and Asp14 were reduced from 2.3 to 1.9 Å. In no case was an upper bound provided. A similar protocol has recently been described by Chazin and co-workers (Akke et al., 1992). (iii) A final set of DG structures was calculated as in step ii with the addition of an upper bound of 2.8 Å for the three predicted peptide–sulfur hydrogen bonds in the metal-binding site (H_N···S—Zn; Table VII and Figure 10). Such refinement is not necessary in the case of peptide hydrogen bonds related to secondary structure, since in the latter case redundancy of NOE and *J*-coupling constraints implicitly impose an upper bound between the amide donor and carbonyl acceptor.

RESULTS

The present studies are based on the solution structure of ZFY-6 (Kochoyan et al., 1991a,b), which contains tyrosine as its central aromatic residue (Tyr10; Figure 2A). Analogues ZFY-*phe* and ZFY-*his* contain amino acid substitutions Tyr10Phe and Tyr10His, respectively (Figure 2A). Our results are presented in three parts. Spectroscopic studies are presented in part I and demonstrate qualitative similarities and differences among analogues in structure and stability. Molecular models are obtained in part II by distance-geometry/simulated annealing (DG/SA) reconstruction. ZFY-*phe* and ZFY-*his* are shown to retain the $\beta\beta\alpha$ motif and to share staggered-horizontal stacking between the variant aromatic residues and the proximal histidine. Protein dynamics are probed in part III by amide proton exchange in D_2O, temperature-dependent conformational broadening, and analysis of the conformational averaging of $^3J_{\alpha NH}$ coupling constants.

(I) Spectroscopic Studies of ZFY-phe and ZFY-his

Relative pH Stabilities of Analogues. Far-UV CD spectra of Zn finger peptides obtained in the absence and presence of Zn^{2+} provide evidence of metal-dependent folding (Frankel et al., 1987; Parraga et al., 1988). Because protonation of the histidine and cysteate side chains under acidic conditions leads to dissociation of Zn^{2+} with unfolding of the peptide, the pH dependence of the mean residue ellipticity at 222 nm ($[\theta]_{222}$) provides a probe to assess relative differences in thermodynamic stability (Weiss et al., 1990; Weiss & Keutmann, 1990). Whereas ZFY-6 and ZFY-*phe* exhibit similar stabilities (midpoint 4.0), the pH stability of ZFY-*his* is reduced (midpoint 4.5) (data not shown). Such reduction may reflect an intrinsic decrease in the thermodynamic stability of the folded state (in which His10 is presumably uncharged) and/or an increase in the relative thermodynamic stability of the unfolded state under acidic conditions (in which His10 would be charged). Inspection of the ^{1}H-NMR spectrum of ZFY-*his* as a function of pH demonstrates that His10 does not titrate in the folded state (i.e., apparent $pK < 4.5$; data not shown). The reduced pH stability of ZFY-*his* is consistent with the decreased pH stability of ZFY domain 8 relative to domain 6 or 10 (Weiss et al., 1990).

NMR Studies of ZFY Analogues. One-dimensional ^{1}H-NMR spectra (amide and aromatic regions in H_2O) of ZFY-6 (spectrum a), ZFY-*phe* (spectrum b), and ZFY-*his* (spectrum c) are shown in Figure 2B. In the presence of equimolar Zn^{2+} each spectrum exhibits a similar range of chemical shifts. Sequential assignment of ZFY-*phe* and ZFY-*his* is obtained as described for the parent peptide (Kochoyan et al., 1991a). The "fingerprint" regions of the NOESY spectra of ZFY-*phe* and ZFY-*his* (containing $d_{\alpha N}$ sequential cross peaks; Wuthrich, 1986) are shown in Figure 3 (panels A and B, respectively). Helix-related ($i,i+3$) contacts are observed in this region as indicated by arrows in the figure. Sequence-specific resonance assignments are given in Tables I (ZFY-*phe*) and II (ZFY-*his*).

Sequence-Specific Resonance Assignment. Sequential and medium-range NOEs, selected ^3J-coupling constants, and slowly exchanging amide resonances for ZFY-*phe* and ZFY-*his* are shown in schematic form in Figure 4 (panels A and B, respectively). These data demonstrate that ZFY-*phe* and ZFY-*his* share the $\beta\beta\alpha$ secondary structural motif (Berg, 1988; Lee et al., 1989a,b) as previously observed in ZFY-6 (Kochoyan et al., 1991a) and other classical Zn fingers (Klevit et al., 1990; Omichinski et al., 1990). Close packing between the N-terminal β-hairpin and C-terminal α-helix is demonstrated by the presence of long-range NOE contacts; in each case these include side-chain contacts Tyr3–Leu18, Tyr7–Ile22, and Ar10–Leu18 (Figure 5). An extensive set of observed β-hairpin/α-helix interactions defines a hydrophobic core (residues Cys5, Cys8, Ar10, Leu18, His21, and H25), which is similar to that observed in ZFY-6 (Kochoyan et al., 1991a,b). Unlike Tyr10 in the spectrum of the parent peptide, the aromatic resonances of Phe10 and His10 are well resolved (Tables I and II), and so selective isotopic labeling is not required to resolve ambiguous NOEs (Kochoyan et al., 1991b).

Comparison of ^{1}H-NMR Chemical Shifts. Significant differences in chemical shifts between analogues (>±0.1 ppm relative to ZFY-6; Kochoyan et al., 1991a) are given in Tables III (ZFY-*phe*) and IV (ZFY-*his*). Sites of chemical shift differences in the spectrum of ZFY-*phe* are localized in space relative to the position of Tyr10 in ZFY-6 (Kochoyan et al., 1991b). More extensive differences in chemical shift are observed in the spectrum of ZFY-*his*; such differences may reflect either an intrinsic change in the geometry of the imidazole ring current relative to that of tyrosine (Johnson & Bovey, 1957) or nonlocal perturbations in protein structure or dynamics (see below). In each case the ring resonances of the central aromatic residue exhibit upfield secondary shifts [as calculated using the random-coil values given by Wuthrich (1986)]: Tyr10, $\Delta H_{2,6} = 0.73$ ppm and $\Delta H_{3,5} = 0.44$ ppm; Phe10, $\Delta H_{2,6} = 0.68$ ppm and $\Delta H_{3,5} = 0.45$ ppm; and His10, $\Delta H_\epsilon = 0.38$ ppm and $\Delta H_\delta = 1.29$ ppm. Such shifts are presumably due in each case to the ring current of the His21–Zn^{2+} complex. Qualitative similarities are also seen in the upfield secondary shifts of Ser15-H_α and Lys25-$H_{\beta 12,\gamma 12}$ and nondegeneracy of the two Gln4-H_γ resonances. Similar trends in chemical shifts are observed in ^{1}H-NMR spectra of unrelated fingers (Lee et al., 1989b; Klevit et al., 1990; Omichinski et al., 1990) and may reflect common features of the $\beta\beta\alpha$ motif.

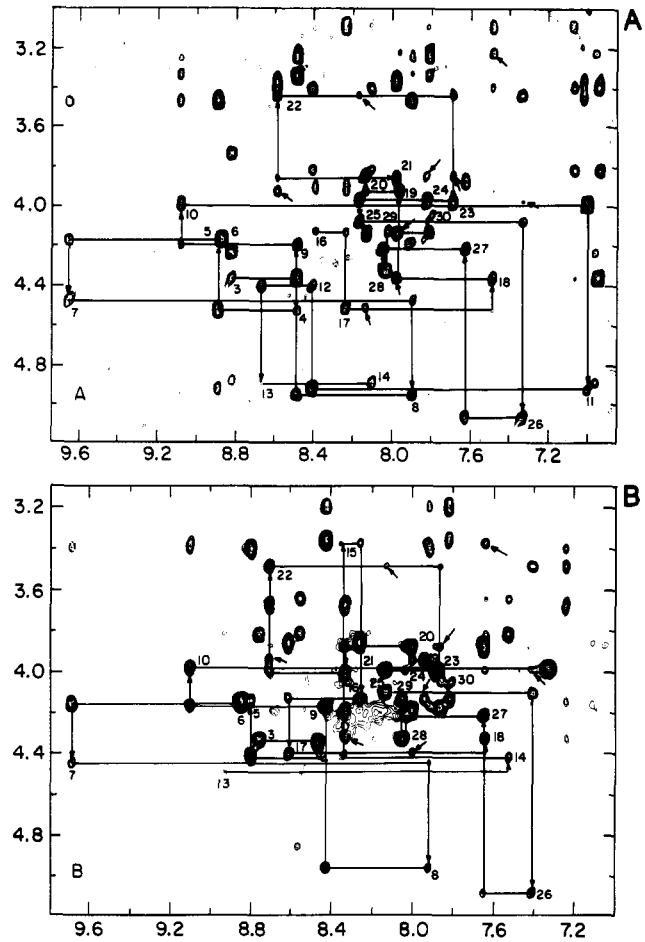

FIGURE 3: Fingerprint regions of the NOESY spectra in H_2O of ZFY-*phe* (A) and ZFY-*his* (B) showing $d_{\alpha N}$ connectivities and sequential assignment. Arrows indicate helix-related ($i,i+3$) contacts.

Comparison of NOESY Spectra. Although NOESY spectra of ZFY-*phe* and ZFY-*his* exhibit detailed similarities to that of the parent peptide (Kochoyan et al., 1991a), some differences are also observed. (i) In the case of ZFY-*phe* a small difference is observed in the relative intensities of NOEs from Phe10 to Ser12 and Leu18 relative to analogous NOEs from Tyr10 to Ser12 and Leu18; this difference is likely to reflect a local change in ring orientation as described below. More extensive differences are observed in the case of ZFY-*his*. Whereas long-range β-sheet-related NOEs in ZFY-*phe*

Table I: Chemical Shifts of the Assigned ^{1}H-NMR Resonances of ZFY-*phe* at pH 5.9

residue	chemical shifts at 25 °C			
	NH	$C^{\alpha}H$	$C^{\beta}H$	others
K1		3.84	1.69, 1.63	$C^{\gamma}H$ 1.04, 1.04; $C^{\delta}H$ 1.52, 1.52; $C^{\epsilon}H$ 2.75, 2.75
T2	8.14	4.25	3.74	$C^{\gamma}H_3$ 0.93
Y3	8.83	4.36	2.84, 2.74	$C^{\delta}H$ 6.97; $C^{\epsilon}H$ 6.72
Q4	8.48	4.53	1.92, 1.86	$C^{\gamma}H$ 2.11, 2.26
C5	8.88	4.17	3.49, 2.76	
Q6	8.86	4.20	1.59, 1.59	$C^{\gamma}H$ 1.50, 1.64
Y7	9.65	4.50	2.56, 1.21	$C^{\delta}H$ 6.82; $C^{\epsilon}H$ 6.68
C8	7.90	4.94	3.35, 3.25	
E9	8.47	4.19	2.02, 1.85	$C^{\gamma}H$ 2.15, 2.25
F10	9.08	4.0	2.80, 2.17	$C^{\delta}H$ 6.62; $C^{\epsilon}H$ 6.94; $C^{\zeta}H$ 7.08
R11	6.99	4.92	1.55, 1.32	$C^{\gamma}H$ 1.47, 1.47; $C^{\delta}H$ 2.99, 2.99
S12	8.40	4.42	3.83, 3.41	
A13	8.66	4.86	1.43, 1.43	
D14	8.10	4.87	2.69, 2.56	
S15	8.63	3.22	3.42, 3.10	
S16	8.38	4.13	3.93, 3.93	
N17	8.22	4.52	3.11, 2.89	
L18	7.47	4.34	2.06, 1.46	$C^{\gamma}H$ 1.75; $C^{\delta}H_3$ 1.05, 0.96
K19	7.95	3.93	1.95, 1.95	$C^{\gamma}H$ 1.40, 1.40; $C^{\delta}H$ 1.62, 1.62; $C^{\epsilon}H$ 2.90, 2.90
T20	8.12	3.85	4.15	$C^{\gamma}H_3$ 1.18
H21	7.98	3.87	3.40, 2.47	$C^{\delta 2}H$ 7.04; $C^{\epsilon 2}H$ 7.47
I22	8.58	3.44	1.93	$C^{\gamma}H_3$ 1.02; $C^{\gamma}H$ 2.20, 1.55; $C^{\delta}H_3$ 1.15
K23	7.68	3.97	1.85, 1.85	$C^{\gamma}H$ 1.42, 1.42; $C^{\delta}H$ 1.59, 1.59; $C^{\epsilon}H$ 2.87, 2.87
T24	7.81	3.98	3.95	$C^{\gamma}H_3$ 1.13
K25	8.16	4.08	0.66, 0.48	$C^{\gamma}H$ 0.91, 0.91; $C^{\delta}H$ 1.35, 1.35; $C^{\epsilon}H$ 2.83, 2.83
H26	7.33	5.04	2.91, 2.66	$C^{\delta 2}H$ 6.57; $C^{\epsilon 2}H$ 7.82
S27	7.63	4.21	3.88, 3.88	
K28	8.05	4.33	1.81, 1.57	$C^{\gamma}H$ 1.27, 1.27; $C^{\delta}H$ 1.47, 1.47
E29	8.01	4.13	1.92, 1.68	$C^{\gamma}H$ 2.02, 2.02
K30	7.80	4.06	1.75, 1.65	$C^{\gamma}H$ 1.31, 1.31; $C^{\delta}H$ 1.58, 1.58; $C^{\epsilon}H$ 2.92, 2.92

Table II: Chemical Shifts of the Assigned ^{1}H-NMR Resonances of ZFY-*his* at pH 6.0

residue	chemical shifts at 25 °C			
	NH	$C^{\alpha}H$	$C^{\beta}H$	others
K1		3.87	1.70, 1.65	$C^{\gamma}H$ 1.07, 1.07; $C^{\delta}H$ 1.53, 1.53; $C^{\epsilon}H$ 2.75, 2.75
T2	8.10	4.35	3.84	$C^{\gamma}H_3$ 0.97
Y3	8.76	4.37	2.76, 2.58	$C^{\delta}H$ 6.88; $C^{\epsilon}H$ 6.71
Q4	8.48	4.44	1.88, 1.84	$C^{\gamma}H$ 2.07, 2.25
C5	8.81	4.16	3.41, 2.63	
Q6	8.86	4.19	1.62, 1.62	$C^{\gamma}H$ 1.48, 1.48
Y7	9.70	4.48	2.52, 1.21	$C^{\gamma}H$ 6.84; $C^{\epsilon}H$ 6.70
C8	7.94	4.94	3.36, 3.20	
E9	8.44	4.20	2.12, 2.02	$C^{\gamma}H$ 2.23, 2.27
H10	9.11	4.0	2.86, 2.22	$C^{\delta}H$ 5.85; $C^{\epsilon}H$ 7.74
R11	7.35	4.82	1.50, 1.29	$C^{\gamma}H$ 1.39, 1.39; $C^{\delta}H$ 3.02, 3.02
S12	8.57	4.55	3.82, 3.65	
A13	8.94	4.53	1.41, 1.41	
D14	7.54	4.46	2.73, 2.73	
S15	8.36	3.38	3.60, 3.60	
S16	8.27	4.15	3.87, 3.87	
N17	8.62	4.43	2.88, 2.82	
L18	7.66	4.34	1.97, 1.44	$C^{\gamma}H$ 1.78; $C^{\delta}H_3$ 0.98, 0.93
K19	7.96	3.96	1.95, 1.95	$C^{\gamma}H$ 1.41, 1.41; $C^{\delta}H$ 1.63, 1.63; $C^{\epsilon}H$ 2.92, 2.92
T20	8.02	3.89	4.21	$C^{\gamma}H_3$ 1.18
H21	8.35	4.04	3.68, 2.89	$C^{\delta 2}H$ 7.24; $C^{\epsilon 2}H$ 7.48
I22	8.71	3.50	1.93	$C^{\gamma}H_3$ 1.02; $C^{\gamma}H$ 2.23, 1.54; $C^{\delta}H_3$ 1.14
K23	7.88	4.02	1.86, 1.86	$C^{\gamma}H$ 1.42, 1.42; $C^{\delta}H$ 1.60, 1.60; $C^{\epsilon}H$ 2.85, 2.85
T24	7.90	4.01	4.01	$C^{\gamma}H_3$ 1.14
K25	8.14	4.13	0.71, 0.53	$C^{\gamma}H$ 0.94, 0.94; $C^{\delta}H$ 1.36, 1.36; $C^{\epsilon}H$ 2.84, 2.84
H26	7.42	5.06	2.90, 2.67	$C^{\delta 2}H$ 6.58; $C^{\epsilon 2}H$ 7.84
S27	7.66	4.24	3.89, 3.89	
K28	8.05	4.36	1.79, 1.54	$C^{\gamma}H$ 1.25, 1.25; $C^{\delta}H$ 1.44, 1.44; $C^{\epsilon}H$ 2.83, 2.83
E29	8.07	4.15	1.92, 1.69	$C^{\gamma}H$ 2.04, 2.04
K30	7.83	4.07	1.74, 1.65	$C^{\gamma}H$ 1.30, 1.30; $C^{\delta}H$ 1.60, 1.60; $C^{\epsilon}H$ 2.92, 2.92

are identical to those of the parent peptide (Kochoyan et al., 1991a), ZFH-*his* does not exhibit expected contacts between Ala13-H_{α} and the H_{α} and γCH_3 of T2, between Tyr3-ortho and Ala13-βCH_3, and between R11-H_{β} and Gln4-H_{α}. Other β-sheet-related and long-range contacts are nevertheless retained (Tyr3-H_N/Ser12-H_N, Tyr3-meta/Asp14-H_{α}, Tyr3-ortho,meta/Ser15-H_{α}, Tyr3-$H_{\beta,\delta}$/Leu18-δCH_3, and Cys5-H_N/His10-$H_{N,\beta,\delta}$), however, which with one exception are sufficient to define an analogous cross-strand hydrogen-bonding scheme (Table VI; see below). The spectrum of ZFY-

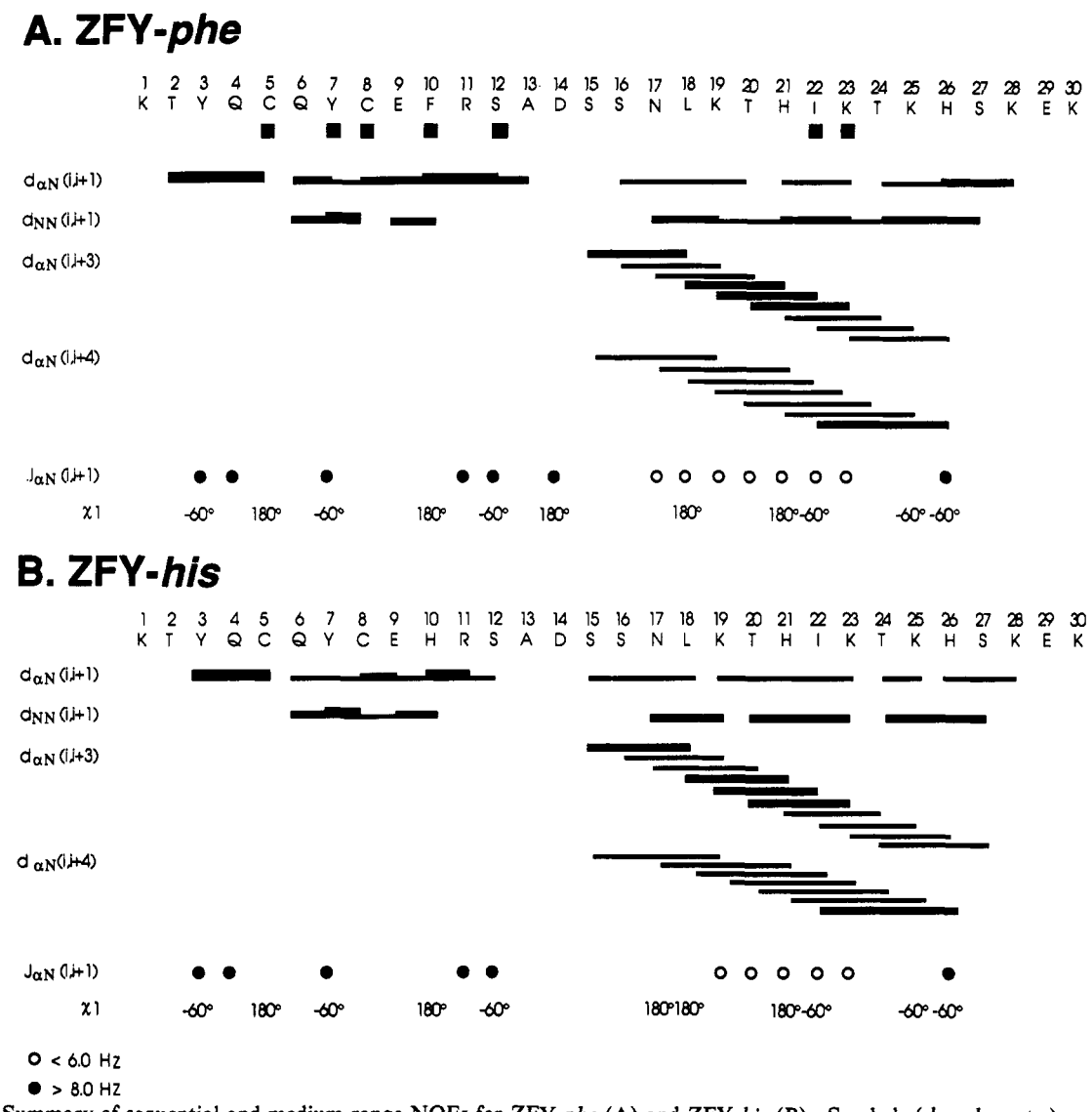

FIGURE 4: Summary of sequential and medium-range NOEs for ZFY-*phe* (A) and ZFY-*his* (B). Symbols ($d_{\alpha N}$, d_{NN}, etc.) are as defined by Wuthrich (1986). Slowly exchanging amide resonances are indicated by closed boxes in the upper panel; these are observed in the spectrum of ZFY-*phe* at 25 °C and of ZFY-*his* at 4 °C. Relative intensity of NOEs is indicated schematically by the thickness of the line. Large and small $^3J_{\alpha N}$ values are indicated by closed and open circles, respectively; χ_1 values are indicated for residues for which stereospecific assignment of β resonances was obtained.

his also exhibits a weak NOE (T2-γCH_3/R11-H_γ) that is not seen in the native domain, which may represent a transient contact between flexible side chains as discussed below. (ii) Whereas both ortho and meta resonances of Tyr10 and F12 exhibit NOEs to His21 and Leu18, such NOEs are observed to His10 H_δ but not His10-H_ϵ. Such side-specific NOEs define a preferred orientation of the imidazole ring in the hydrophobic core and demonstrate hindered rotation about the C_β–C_γ bond axis. (iii) No NOEs are observed between His10 and Ser12. The distinct NOE pattern of His10 may in part reflect the different placement of protons on an imidazole ring and in part differences in side-chain position (part II). (iv) In ZFY-6 and ZFY-*phe* the side-chain configuration of Asp14 is well-defined by stereospecific assignment of the β resonances and medium-strength NOEs to the amide resonance of Asn17. As discussed below, this configuration is consistent with formation of an N-cap hydrogen bond between the Asp14 γ-carboxylate and the Asn17 amide proton. In the spectrum of ZFY-*his* the β resonances are degenerate and exhibit weak multiple NOEs to the amide resonances of residues 15, 16, and 17. The dynamic implications of this observation are considered in part III.

(II) Solution Structures of ZFY-phe and ZFY-his

Twenty DG/SA calculations were initiated for each analogue; of these, 16 converged for ZFY-*phe* and 15 converged for ZFY-*his*. Models of ZFY-*phe* (Figure 6B) were obtained on the basis of 176 NOE restraints (76 sequential, 45 medium range, and 50 long range) and 24 dihedral restraints; models of ZFY-*his* (Figure 6C) were obtained on the basis of 187 NOE restraints (89 sequential, 47 medium range, and 45 long range) and 23 dihedral restraints (supplementary material). Analogous restraints were previously obtained for the parent peptide (Kochoyan et al., 1991a,b). The maximum NOE restraint violation in the ZFY-*phe* ensemble was 0.14 Å and in the ZFY-*his* ensemble was 0.10 Å. The most consistent DG/SA model of ZFY-*phe* contained two NOE violations between 0.05 and 0.06 Å and 13 NOE violations less than 0.05 Å. The most consistent DG/SA model of ZFY-*his* contained one NOE violation of 0.06 Å and seven NOE violations less than 0.05 Å. For each analogue the distributions of backbone dihedral angles (ϕ, ψ) cluster in the expected regions of the Ramachandran plot as shown in the supplementary material. Statistical parameters

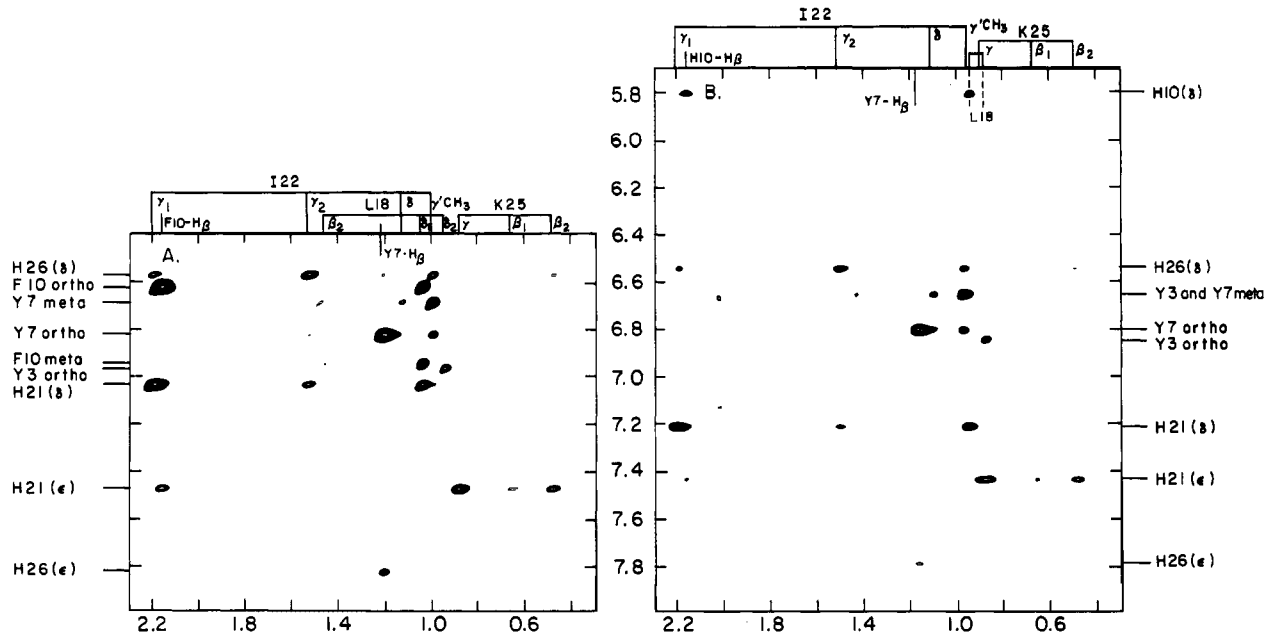

FIGURE 5: Long-range NOEs observed in the NOESY spectra of ZFY-*phe* (A) and ZFY-*his* (B). The region shown contains contacts between aromatic and aliphatic protons (conditions: 25 °C, mixing time 200 ms, pD 6.0 in D_2O, direct meter reading).

Table III: Chemical Shift Difference of ZFY-*phe* and ZFY-6 at 25 °C (>0.1 ppm)

	chemical shifts			
residue	NH	$C^{\alpha}H$	$C^{\beta}H$	others
R11				$C^{\delta}H$ −0.31, −0.31
D14	−0.11			
N17		0.1	−0.16	
H21	−0.28		−0.15, −0.13	

Table IV: Chemical Shift Difference of ZFY-*his* and ZFY-6 at 25 °C (>0.1 ppm)

	chemical shifts			
residue	NH	$C^{\alpha}H$	$C^{\beta}H$	others
T2		0.10		
Y3			−0.17	
Q4		−0.11		
C5			−0.12	
Q6				$C^{\gamma}H$ −0.22
E9			0.10, 0.14	$C^{\gamma}H$ 0.10
R11	0.44	−0.10		$C^{\delta}H$ −0.28, −0.28
S12	0.18	0.10	0.22	
A13	0.29	−0.37		
D14	−0.67	−0.42	0.1	
S15	−0.29	0.13	0.20, 0.56	
N17	0.45		−0.17, −0.23	
L18	0.17			
H21		0.12	0.13, 0.29	$C^{\delta}H$ 0.13
K23	0.16			

describing the DG/SA ensembles are provided in Table V. The overall average of main-chain rms differences (calculated on the basis of pairwise alignment of the main-chain atoms of residues 2–27) *between* ensembles is similar to those *within* a single ensemble (0.5–0.6 Å).

Each analogue retains the $\beta\beta\alpha$ motif and folds as a globular minidomain as in canonical Zn fingers (Lee et al., 1989a,b; Omichinski et al., 1990; Klevit et al., 1990). In Figure 6 are shown ensembles of 12 DG/SA structures for ZFY-6, ZFY-*phe*, and ZFY-*his* (panels A–C, respectively) with selected side chains in the hydrophobic core (Ar10, Ser12, Leu18, His21, and His26). In Figure 6D is shown a superposition of backbone configurations of ZFY-6 (red) and ZFY-*phe* (green); the ensembles are aligned according to the backbone atoms of residues 21–26 (i.e., the invariant HX_4H metal-binding site). A corresponding alignment of ZFY-6 (red) and ZFY-*his* (blue) is given in panel E. In each hydrophobic core displaced-horizontal stacking (Burley & Petsko, 1988) is observed between the swapped aromatic residue (Ar10) and proximal histidine (His21); the C-terminal helix partitions between an α-helical portion (residues 15–20) and the nonstandard HX_4H helix with characteristic bifurcating hydrogen bonds (residues 21–27; Table VI). These features, which distinguish even (nonconsensus) and odd (consensus) ZFY domains, were previously described in the refined structure of ZFY-6 (Kochoyan et al., 1991b). Hydrogen bonds corresponding to slowly exchanging amide resonances are indicated by asterisks in Table VI. In each analogue bidentate hydrogen bonds are possible but not established between the Gln4 side-chain amino group and the main-chain carbonyl oxygens of Cys5 and Glu9 (Figure 8A). Formation of such hydrogen bonds would rationalize the inequivalent chemical shifts of the two Gln4 H_{δ} resonances (Tables I and II) and is suggested by strong NOEs from Gln4-$H_{\epsilon 1}$ and -$H_{\epsilon 2}$ to the H_N resonances of Cys5 and Glu9. Gln4 is an invariant feature of most even-numbered ZFY domains (Figure 1) but is otherwise unusual among consensus Zn fingers (Gibson et al., 1988). Further investigation of possible side-chain hydrogen bonds will require a high-resolution solution structure (Omichinksi et al., 1990).

A small shift is observed in Phe10 relative to Tyr10 or His10, reflecting input of a tighter restraint to one of the β protons of Ser12 in the Phe10 DG calculation. This has the effect of decreasing the solvent accessibility of the Phe10 para proton (mean normalized solvent accessibility 14%) relative to that of the Tyr10 *p*-OH group (mean normalized solvent accessibility 31%). It is also possible that the detailed configuration of the aromatic rings is influenced by hydrogen bonding between Ser12 γOH and Tyr10 *p*-OH (ZFY-6) or between Ser12 γOH and His10 N_{δ} (ZFY-*his*), which would not be possible in ZFY-*phe*. Although such Tyr10 and His10 hydrgen bonds cannot be directly observed by ^{1}H-NMR, in the majority of Tyr10 structures and in the minority of His10 structures they are allowed following rotation of Ser12 γOH.

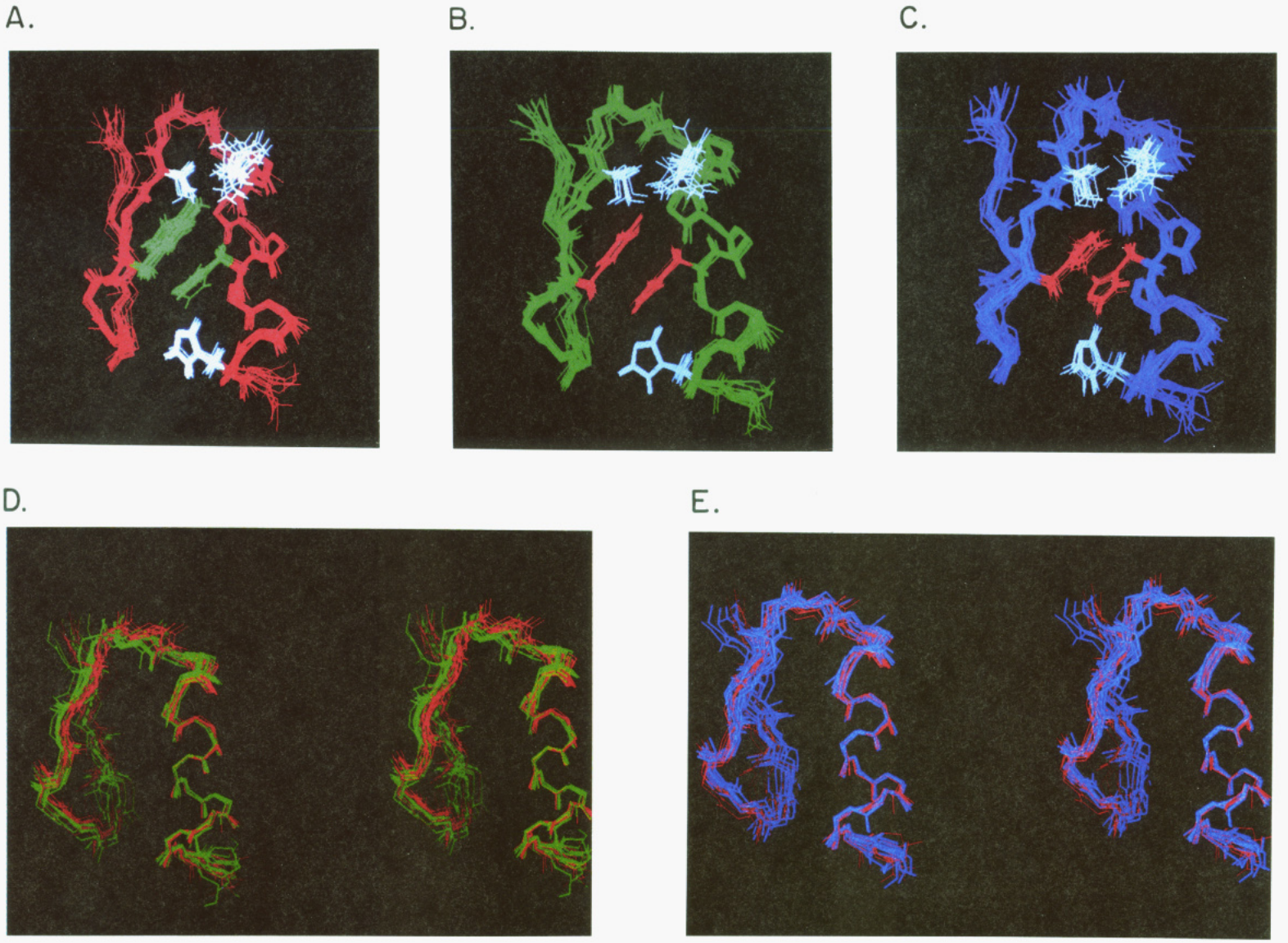

FIGURE 6: (A) DG/SA ensemble of the parent peptide (ZFY-6; Kochoyan et al., 1991a,b). The backbone is shown in red; selected side chains are shown clockwise from the center left in alternating colors: Tyr10 (green), Ser12 (white), Leu18 (white), His21 (green), and His26 (white, bottom right). The side chains of Tyr10 and His21 are in green, and the side chains of Ser12, Leu18, and His26 are in white. The β-OH of Ser12 is well positioned to contribute a hydrogen bond to the Tyr10 *p*-OH. (B) DG/SA ensemble of ZFY-*phe*. The backbone is shown in green, the side chains of Phe10 and His21 are in red, and the side chains of Ser12, Leu18, and His26 are in white. (C) DG/SA ensemble of ZFY-*his*. The backbone is shown in blue, the side chains of His10 and His21 are in red, and the side chains of Ser12, Leu18, and His26 are in white. (D) Stereo comparison of the backbone structures of ZFY-6 (red) and ZFY-*phe* (green). (E) Stereo comparison of the backbone structures of ZFY-6 (red) and ZFY-*his* (blue). In panels A–C the structures are aligned according to the main-chain atoms of residues 3–26; in panels D and E the respective families of structures are aligned according to the main-chain atoms of residues 21–26 (the invariant HX_4H metal-binding site).

Table V: Statistical Parameters Describing NMR Ensembles[a]

	ZFY-*his*	ZFY-*phe*	ZFY-6T
(A) rms deviations (excluding disordered regions)[b]			
main chain (Å)	0.58	0.56	0.50
side chains (Å)	1.53	1.49	1.42
(B) average NOE restraint violations[c]			
upper-bound violations (Å)	0.018	0.020	0.014
(C) deviations from ideal covalent geometry			
bond lengths (Å)	0.11	0.10	0.12
bond angles (deg)	3.4	3.2	3.4

[a] In each case the ensembles were calculated assuming S–H_N distances of 2.2–2.8 Å for the Cys5–Tyr7, Cys5–Cys8, and Cys8–Ar10 sulfur–amide hydrogen bonds (see Materials and Methods). [b] NMR ensembles were aligned in each case according to the C^α positions of residues 3–26; rms values shown correspond to these regions. [c] NOE restraint violations represent rms upper-bound violations; no lower bounds were assumed.

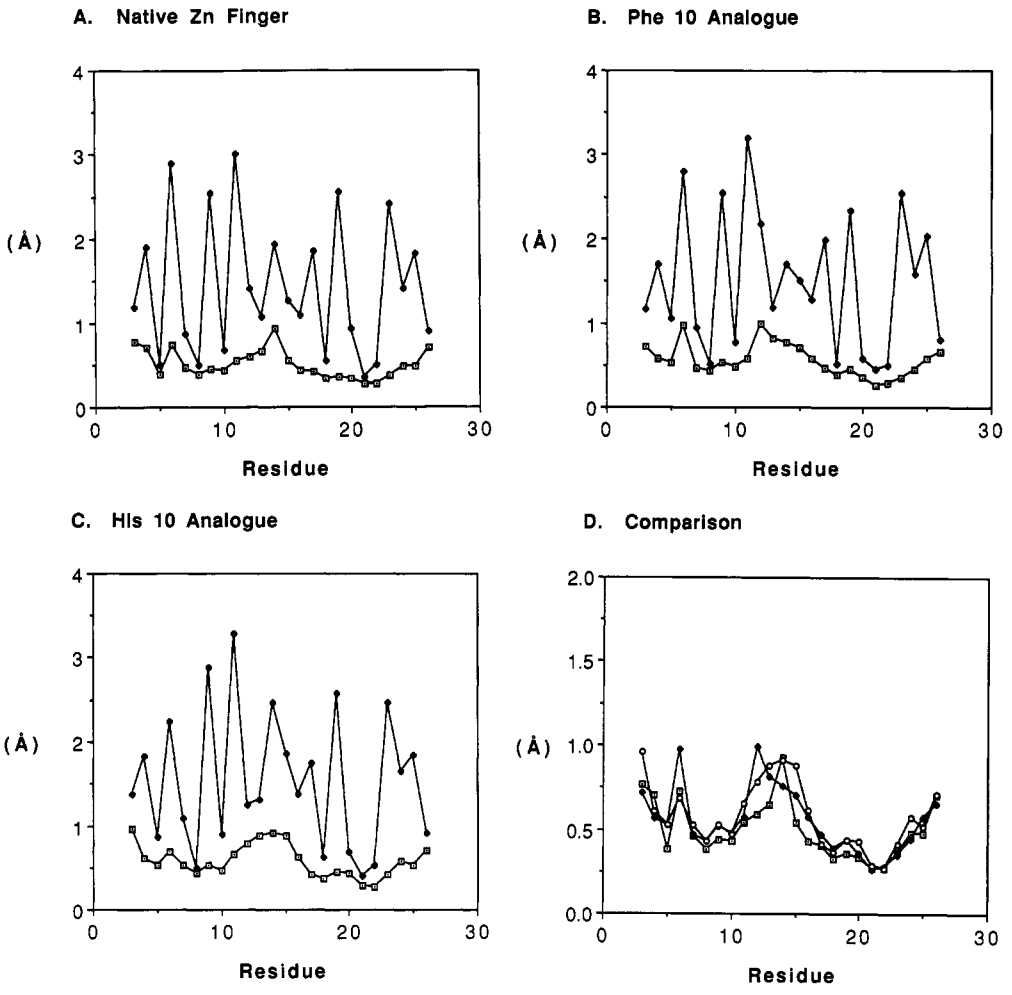

FIGURE 7: rms deviations shown by residue for the main-chain (□) and side-chain atoms (◆) of ZFY-6 (A), ZFY-*phe* (B), and ZFY-*his* (C). (D) Comparison of main-chain rms deviations for the three analogues: ZFY-6 (□), ZFY-*phe* (◆), and ZFY-*his* (○).

The presence of a hydrogen bond between Ser12 γOH (as donor) and Tyr10 *p*-OH_ζ (as acceptor) has recently been demonstrated by analysis of the tyrosine Fermi vibrational doublet in the laser Raman spectrum of ZFY-6 (T. Li, M. A. Weiss, and G. J. Thomas, Jr., manuscript in preparation). Aspects of the ZFY-*his* ensemble are less precise than corresponding features in the other ensembles. The N-terminal hydrogen bond of the β-sheet (Tyr3 H_N–Ser12 C=O) is not consistently predicted (Table VI), for example, and certain side-chain rms deviations are larger (residues 11, 14, 15, and 16; Figure 7). These reflect differences in the NOESY data (see part I). In the case of Asp14-H_β, which in ZFY-*his* exhibits weak NOEs to the amide resonances of residues 15, 16, and 17, no restraints were introduced as these three contacts cannot simultaneously be satisfied by a single structure. The configuration of Asp14 in ZFY-6 and ZFY-*phe* is consistent with formation of an N-cap hydrogen bond (Richardson & Richardson, 1988) to the amide proton of Asn17 (Figure 8B). The rms deviation of the His10 side chain (0.9 Å) is larger than that of the Tyr10 or Phe10 side chains (0.7 Å); whether this reflects increased mobility or "proton scarcity" is not clear and is discussed further below.

(III) Comparative Studies of Protein Dynamics

Distinguishing between informational and physical uncertainties in the analysis of dispersion in a DG structure is a general problem in NMR spectroscopy. Imprecision is in part technical. The imidizole ring contains fewer protons, for example, than that of phenylalanine or tyrosine and so provides fewer probes with which to define local structure by NOEs (informational uncertainty); other sources of informational uncertainty include chemical shift overlap, coarse interpretation of NOEs (as strong, medium, or weak), and incomplete stereospecific assignment of methylene protons. Fluctuations

Table VI: Predicted Hydrogen Bonds in DG/SA Ensembles[a]

donor	acceptor	no. of structures involved	energy (kcal/mol)	distance (Å)[b]	angle [*D* (deg)][c]
		ZFY-6			
3 N···HN	O=C 12	11	−0.6	3.4	35
5 N···HN*	O=C 10	13	−1.4	3.1	31
10 OH···HH	Oγ 12	8	−0.1	3.0	60
12 N···HN*	O=C 3	14	−0.7	3.3	35
18 N···HN	O=C 14	6	−0.3	3.2	45
19 N···HN	O=C 15	14	−0.6	3.1	37
20 N···HN	O=C 16	13	−1.8	3.3	12
21 N···HN	O=C 17	13	−0.3	3.1	45
22 N···HN*	O=C 18	14	−1.4	3.0	27
23 N···HN*	O=C 19	13	−1.0	2.9	38
24 N···HN*	O=C 20	11	−0.5	3.0	45
24 N···HN	O=C 21	6	−0.0	3.3	43
25 N···HN	O=C 21	9	−0.1	2.9	57
26 N···HN	O=C 22	13	−0.1	3.1	49
		ZFY-*phe*			
3 N···HN	O=C 12	6	−0.4	3.3	43
5 N···HN*	O=C 10	14	−0.7	3.0	44
12 N···HN*	O=C 3	11	−1.0	3.4	34
18 N···HN	O=C 14	5	−0.2	3.2	50
19 N···HN	O=C 15	6	−0.5	3.6	31
20 N···HN	O=C 16	5	−0.3	3.8	15
21 N···HN	O=C 17	14	−0.2	3.0	47
22 N···HN*	O=C 18	14	−1.8	3.0	22
23 N···HN*	O=C 19	14	−0.7	2.9	41
24 N···HN*	O=C 20	14	−0.6	3.0	44
24 N···HN	O=C 21	7	−0.0	3.1	45
25 N···HN	O=C 21	11	−0.3	2.9	55
26 N···HN	O=C 22	13	−0.1	3.1	48
		ZFY-*his*			
3 N···HN	O=C 12	6	−0.4	3.4	50
5 N···HN*	O=C 10	12	−0.7	3.1	43
12 N···HN*	O=C 3	11	−1.1	3.4	25
18 N···HN	O=C 14	6	−0.3	3.6	43
19 N···HN	O=C 15	10	−1.2	3.3	24
20 N···HN	O=C 16	9	−0.7	3.5	22
21 N···HN	O=C 17	12	−0.4	3.2	41
22 N···HN*	O=C 18	14	−1.4	3.0	28
23 N···HN*	O=C 19	14	−0.8	2.9	40
24 N···HN*	O=C 20	12	−1.0	3.1	38
25 N···HN	O=C 21	12	−0.2	3.0	55
26 N···HN	O=C 22	14	−0.1	3.2	47

[a] Presumptive hydrogen bonds are listed only if present in more than 4 out of 14 structures. Carbonyl oxygen acceptors are designated O=C. [b] Distances are between heavy atoms and so differ from those in Table VII. [c] *D* (deg) is defined as deviation from linearity. Asterisks indicate slowly exchanging amide resonances in D_2O.

on a time scale faster than the rotational correlation time (<2 ns) may in principle be directly probed through measurements of heteronuclear relaxation times (Palmer et al., 1991); such comparative studies of ^{15}N- or ^{13}C-labeled Zn finger analogues are of future interest. Here we investigate the dynamics of ZFY analogues by observation of amide–proton exchange rates in D_2O (>minutes), conformational broadening of resonances in intermediate exchange (milliseconds), and temperature-dependent changes in $^3J_{\alpha N}$ coupling constants of resonances in fast exchange (<milliseconds).

(*i*) *Slowly Exchanging Amide Resonances.* In a freshly prepared D_2O solution (25 °C and pD 6.0) the spectrum of ZFY-*phe* contains eight amide proton resonances that slowly exchange over 18 h; these are Cys5, Tyr7, Cys8, Phe10, Ser12, Ile22, K23, and Thr24. The kinetics of exchange are essentially identical to those of ZFY-6 (Kochoyan et al., 1991a). Five of the slowly exchanging amide resonances correspond to hydrogen bonds in the β-sheet (Cys5 and Ser12) or C-terminal helix (Ile22, K23, and Thr24) as indicated in Table VI (asterisks). The amide protons of Tyr7 and Cys8 are well positioned in the metal-binding site to form bifurcating hydrogen bonds with Cys5-S_γ; the amide proton of Phe10 is similarly well positioned to contact Cys8-S_γ (Table VII). The spectrum of ZFY-*his* contains no slowly exchanging amide proton resonances after 20 min at 25 °C (Figure 9). However, the same set of eight slowly exchanging amide resonances are observed at 4 °C (data not shown), consistent with formation of corresponding hydrogen bonds as predicted by DG calculations. These observations support the hypothesis that ZFY-*his* is less stably folded but retains a similar average structure.

We note that (*i*,*i*+2) sulfur–amide hydrogen bonds (Cys5-Sγ/Tyr7-H_N and Cys8-S_γ/Ar10-H_N in the present case) were predicted by Berg (1988) by analogy to X-ray structures of unrelated Zn^{2+} binding sites. Bifurcating Cys5-S_γ sulfur–amide hydrogen bonds were not anticipated and are shown in Figure 10. In each analogue the sulfur–amide hydrogen bonds correspond to the longest-lived amide resonances in D_2O. It is important to emphasize that the three amide–sulfur hydrogen bonds are predicted in the absence of explicit constraints (column A in Table VII) and only subsequently refined by imposing an upper bound on the H_N···S_γ—Zn^{2+} distance (column B). The mechanism of sulfur–amide proton exchange—i.e., whether exchange occurs via the folded or unfolded (Zn^{2+}-free) states—has not been determined in this or other systems. An analysis of amide proton exchange rates in these and other analogues will be published separately (manuscript in preparation).

(*ii*) *Conformational Broadening at Low Temperature.* A striking difference is observed in the temperature dependence of the one-dimensional ^1H NMR spectra of ZFY-*phe* and ZFY-*his* in the range 0–50 °C. Whereas the line widths of Phe10 resonances exhibit the expected degree of broadening with decreasing temperature, the H_δ and H_ϵ resonances of His10 exhibit more extensive line broadening, suggesting an intermediate exchange mechanism (supplementary Figure S2). These observations are independent of pH in the range 6.0–8.0 (data not shown). Although the His10 side chain is presumably in fast exchange under conditions of the structure determination (25 °C), the nature of the two (or more) substrates involved in the exchange process is not clear from the DG calculations. Observations of side-specific ring NOEs (part I; see above) makes it unlikely that pseudo ring flipping (180° ring rotation about the C_β–C_γ bond axis) is responsible. Exchange between neutral and charged states of the imidizole ring is also unlikely, since the intermediate exchange behavior is pH-independent. A possible mechanism is exchange between a state in which the imidizole N_δ receives a hydrogen bond from Ser12-OH_γ (and thus is packed in the hydrophobic core) and a state in which this hydrogen bond is absent. Since the exchange process occurs on a millisecond time scale, such a mechanism would presumably require a coupling between hydrogen bond formation and other structural changes to account for the observed activation barrier between states.

(*iii*) *Temperature Dependence of $^3J_{\alpha N}$ Coupling Constants.* $^3J_{\alpha N}$ values may be different between analogues due to differences in local structure or dynamics. Fluctuations in the configuration of a polypeptide chain that alter φ dihedral angles would be expected to alter in turn observed $^3J_{\alpha N}$ values. Given the shape of the Karplus curve, the largest perturbations would be expected for those residues whose average φ angle corresponds to an extremum of the Karplus curve, e.g., residues in an α-helix ($^3J_{\alpha N}$ < 4.5 Hz for φ −57°) or antiparallel β-sheet ($^3J_{\alpha N}$ > 8 Hz for φ near −139°). Fluctuations in φ

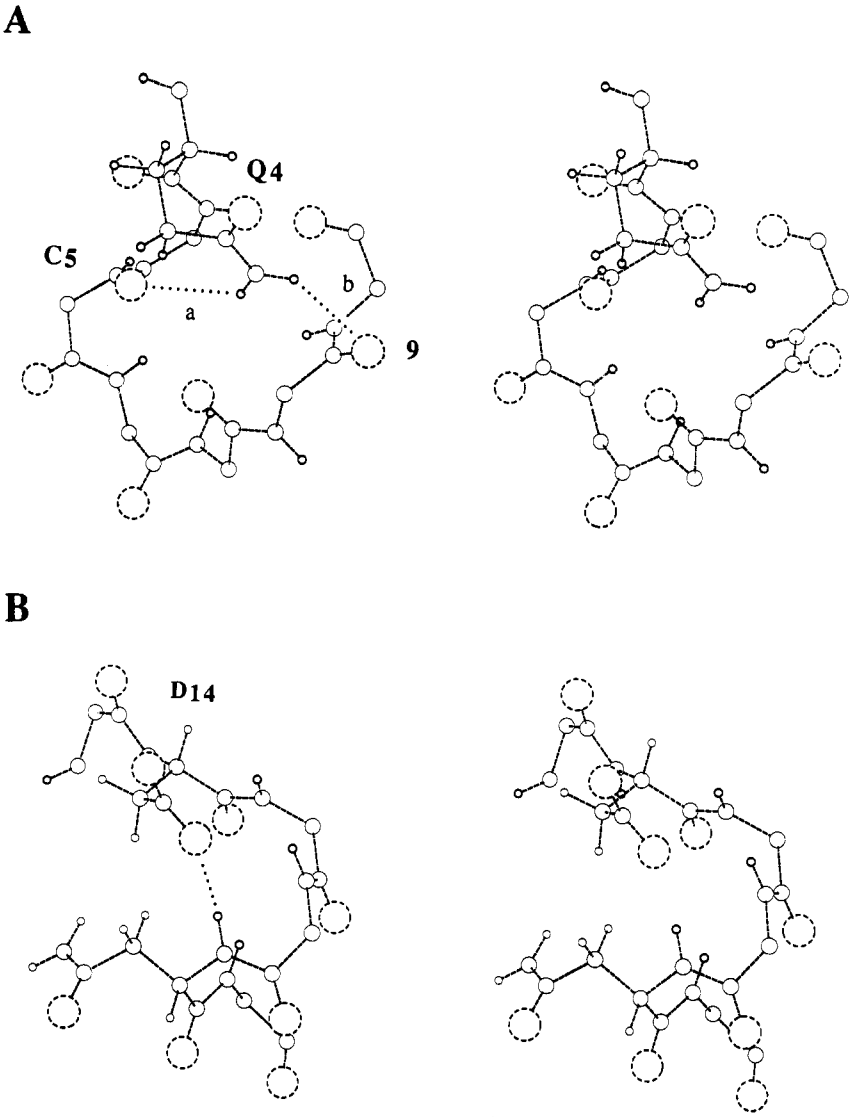

FIGURE 8: (A) Proposed bidentate hydrogen bonds between the side-chain amide protons of Gln4 and the carbonyl oxygens of Cys5 (a) and Glu9 (b). Carbonyl oxygens are shown as larger dashed circles, and amide protons as smaller solid circles. (B) Proposed hydrogen bond in ZFY-6 and ZFY-*phe* between the Asp14 side-chain carboxylate (N-cap; Richardson & Richardson, 1988) and the amide proton of N17.

Table VII: Predicted Hydrogen Bonds between Sulfur and Amide Protons[a]

donor	acceptor	distance (Å)[b]		angle [*D* (deg)][c]	
		A[d]	B[e]	A	B
		ZFY-6			
7 N···HN*	5 S_γ	2.7 ± 0.3	2.5 ± 0.2	30 ± 8	30 ± 11
8 N···HN*	5 S_γ	3.2 ± 0.5	2.8 ± 0.1	33 ± 16	29 ± 14
10 N···HN*	8 S_γ	2.5 ± 0.2	2.4 ± 0.2	36 ± 8	31 ± 11
		ZFY-*phe*			
7 N···HN*	5 S_γ	2.8 ± 0.3	2.6 ± 0.2	31 ± 10	29 ± 10
8 N···HN*	5 S_γ	3.1 ± 0.4	2.7 ± 0.1	30 ± 15	23 ± 13
10 N···HN*	8 S_γ	2.9 ± 0.3	2.6 ± 0.2	51 ± 16	39 ± 15
		ZFY-*his*			
7 N···HN*	5 S_γ	2.7 ± 0.2	2.4 ● 0.1	29 ± 12	26 ± 14
8 N···HN*	5 S_γ	3.1 ± 0.3	2.7 ± 0.2	25 ± 18	17 ± 10
10 N···HN*	8 S_γ	2.7 ● 0.4	2.6 ± 0.2	50 ± 17	49 ± 16

[a] Predicted sulfur-related hydrogen bonds correspond in each case to slowly exchanging amide resonances in D_2O (asterisks). [b] Distance is measured between the amide proton and sulfur; values shown represent ensemble averages. To allow hydrogen bond formation, the minimum (S, H_N) internuclear distance permitted by the DGII program was set to 2.2 Å; the sum of the hydrogen and sulfur hard-sphere radii would otherwise be 2.75 Å. The ± values represent root-mean-square deviations. [c] *D* (deg) is defined as deviation from linearity; values shown represent ensemble averages. [d] In column A the distance between sulfur and hydrogen was restrained to be >2.2 Å; no upper bound was imposed. [e] In column B the selected (S,H_N) distances were constrained between 2.2 and 2.8 Å.

would be expected to increase small $^3J_{\alpha N}$ values and decrease large $^3J_{\alpha N}$ values as more extended regions of the Karplus curve are sampled (Smith et al., 1991). We note that the standard parameters of the Karplus curve are based on studies of BPTI (Pardi et al., 1984) and therefore implicitly incorporate the scale of fluctuations in this reference protein.

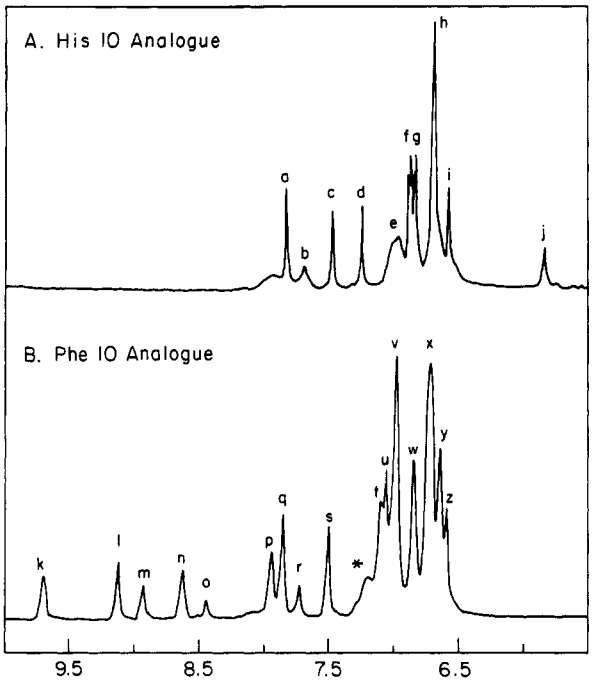

FIGURE 9: Slowly exchanging amide resonances observed in the spectrum of ZFY-*phe* (B) but not in the spectrum of ZFY-*his* (A) after 20 min in D_2O (pD 6.0 and 25 °C). In the former case complete exchange is observed over 18 h; the corresponding set of slowly exchanging amide resonances is observed at 4 °C in the spectrum of ZFY-*his*. Resonances in panel A: (a) His26-H_ϵ, (b) His10-H_ϵ, (c) His21-H_ϵ, (d) His21-H_δ, (e) unassigned, (f) Tyr3-ortho, (g) Tyr7-ortho, (h) overlap of Tyr3- and Tyr7-meta, (i) His26-H_δ, and (j) His10-H_δ. Resonances in panel B: (k) Tyr3-H_N, (l) Phe10-H_N, (m) Cys5-H_N, (n) Ile22-H_N, (o) Ser12-H_N, (p) Cys8-H_N, (q) His26-H_ϵ, (r) K23-H, (s) His21-H_ϵ, (t) Phe10-H_N, (u) His21-H_δ, (v) overlap of Tyr3-ortho and Phe10-meta, (w) Tyr7-ortho, (x) overlap of Tyr3- and Tyr7-meta, (y) Phe10-ortho, and (z) His26-H_δ; an unassigned resonance is indicated by an asterisk.

$^3J_{\alpha N}$ values for ZFY-*phe* and ZFY-*his* at three temperatures are given in Tables VIII and IX, respectively. Although both sets of coupling constants are in qualitative accord with the DG structures, a systematic trend is observed toward increased apparent averaging in ZFY-*his*. For example, at 25 °C $^3J_{\alpha N}$ values of three consecutive α-helical residues, Leu18-Lys19-Thr20, are 5.8, 5.1, and 5.3 Hz, respectively, in ZFY-*phe* but 6.0, 5.3, and 5.8 Hz, respectively, in ZFY-*his*. As would be expected, the difference is more pronounced at 40 °C than at lower temperatures. The $^3J_{\alpha N}$ values of Asp14 are 7.6 (ZFY-*his*) and 9.0 (ZFY-*phe*) at 25 °C; dynamic averaging of this coupling would be in accord with observations above (part I) that in ZFY-*his* the Asp14 β resonances are degenerate and exhibit an inconsistent set of weak NOEs whereas in ZFY-*phe* the two β resonances are resolved and exhibit unique NOEs.

Table VIII: Observed NH–C$^\alpha$H Antiphase Splittings and Corrected $J_{\alpha NH}$ Coupling Constants for ZFY-*phe* at Three Temperatures[a]

	10 °C		25 °C		40 °C	
residue	J_{corr}	J_{obs}	J_{corr}	J_{obs}	J_{corr}	J_{obs}
Tyr3	8.8	9.3	9.4	9.8	9.2	9.6
Glu4	8.4	8.7	8.3	8.7		
Cys5	5.0	5.3	4.9	5.6	5.4	5.9
Gln6	5.8	6.2	5.5	6.3	6.6	6.5
Tyr7	9.6	10.0	9.5	9.8	9.6	9.8
Cys8			6.0	6.4	5.9	6.3
Glu9	5.2	5.5	5.5	6.2	5.5	6.1
Phe10	4.5	4.7	4.5	5.1	4.4	4.8
Arg11			8.6	9.0	8.6	8.9
Ser12	8.1	8.4	8.2	8.6	8.2	8.6
Asp14			9.0	9.3	9.0	9.2
Ser16	5.3	5.8	6.0	6.8	7.2	7.7
Asn17	5.6	5.9	5.7	6.3		
Leu18	5.9	6.3	5.8	6.3	5.4	5.9
Lys19			5.1	5.5	4.7	5.3
Thr20	4.8	5.1	5.3	5.9	5.2	5.8
His21			5.0	5.6	4.9	5.5
Ile22	4.5	4.7	5.1	5.9	4.9	5.4
Lys23	4.9	5.2	5.2	5.8	5.1	5.7
Thr24	6.1	6.5	6.7	7.3	6.7	7.1
Lys25	7.6	7.9	7.9	8.4	7.9	8.3
His26	9.4	9.4	9.7	9.9	9.9	10.1
Ser27	5.3	5.6	5.8	6.3	7.1	7.7
Lys28	7.3	7.7	7.6	8.0	8.1	9.0

[a] Line-width corrections were applied and estimates of true coupling constants obtained from DQF-COSY multiplets by the method of Redfield and Dobson (1991).

DISCUSSION

The classical Zn finger, a conserved module of protein–DNA recognition (Klug & Rhodes, 1987; Pavletich & Pabo, 1991), provides a model for analysis of metal-dependent protein folding (Frankel et al., 1987; Parraga et al., 1988). Conserved or invariant residues define a sequence template that encodes a characteristic structure (the $\beta\beta\alpha$ motif; Lee et al., 1989a,b; Omichinski et al., 1990; Klevit et al., 1990; Kochoyan et al., 1991a). Because of its small size, the informational content of this template (Bowie et al., 1990) may be dissected by peptide mutagenesis (Parrage et al., 1990; Weiss & Keutmann, 1990).

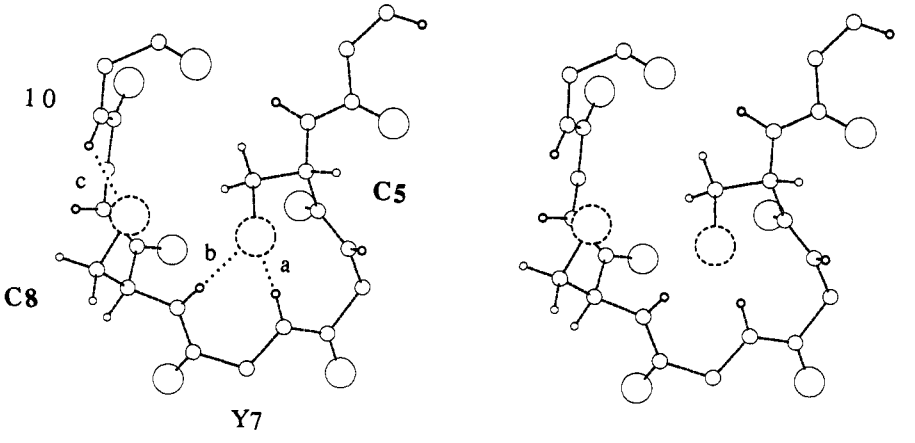

FIGURE 10: Proposed hydrogen bonds between sulfur (dashed circle) and amide protons in the metal-binding site: (a and b) bifurcating hydrogen bonds between Cys5-S_γ and the H_N protons of residues 7 and 8; (c) single hydrogen bond between Cys8-S_γ and the H_N of residue 10.

Table IX: Observed NH–C$^{\alpha}$H Antiphase Splittings and Corrected $J_{\alpha NH}$ Coupling Constants for ZFY-*his* at Three Temperatures[a]

	10 °C		25 °C		40 °C	
residue	J_{corr}	J_{obs}	J_{corr}	J_{obs}	J_{corr}	J_{obs}
Tyr3	9.7	10.1	9.5	9.8	9.4	9.9
Glu4	8.0	9.3	8.1	8.6	7.0	7.6
Cys5	5.9	7.0	6.0	6.7	5.6	6.5
Gln6	7.8	8.6	6.3	7.1	6.5	7.2
Tyr7	9.4	10.2	9.4	9.9	8.9	9.8
Cys8			6.3	6.9	6.5	7.1
Glu9	6.3	7.8	6.5	7.2	6.3	7.1
His10			5.1	5.2		
Arg11			8.9	13.6	9.3	10.1
Ser12	8.0	8.6	8.7	9.2		
Asp14	9.4	9.5	7.6	8.1		
Ser16	5.4	6.6	6.1	6.6	7.6	8.7
Asn17			7.1	7.6		
Leu18			6.0	6.9	6.1	7.8
Lys19			5.3	6.1	5.3	6.1
Thr20	5.8	6.6	5.8	6.3	5.9	6.5
His21			5.1	5.6	5.5	6.4
Ile22	4.8	6.0	5.5	6.3	5.7	6.3
Lys23	4.7	6.6				
Thr24	6.2	7.3	6.5	7.3	7.4	8.2
Lys25	8.3	8.9	7.7	8.2	7.7	8.2
His26	9.4	9.7	9.7	10.0	9.7	10.1
Ser27	6.2	7.0	6.1	6.6	6.3	7.3
Lys28	7.9	8.5	8.0	8.4	7.7	8.5

[a]Line-width corrections were applied and estimates of true coupling constants obtained from DQF-COSY multiplets by the method of Redfield and Dobson (1991).

In this and previous studies (Weiss et al., 1990; Weiss & Keutmann, 1990; Kochoyan et al., 1991a–d) we have focused on the alternating Zn finger motifs observed in the ZFY-related family. Whereas odd-numbered ZFY domains are consensus Zn fingers, even-numbered domains exhibit systematic sequence differences (Page et al., 1987). Structural characterization of such variant sequences may provide insight into general features of the Zn finger motif. Of particular interest is the central aromatic residue, which alternates between position 12 (consensus) or position 10 (swapped; Kochoyan et al., 1991c). 2D-NMR studies of representative analogues demonstrate that both F12 and Tyr10 pack into the hydrophobic core of the domain and provide similar contributions to its thermodynamic stability (Weiss & Keutmann, 1990; Kochoyan et al., 1991c; Mortishire-Smith et al., 1992). The present study is motivated by an apparent difference in the structural role of central and swapped aromatic residues, as suggested by patterns of sequence conservation or divergence in the ZFY gene family (DiLella et al., 1990). Whereas F12 is invariant among odd-numbered domains (and, more generally, among most consensus Zn fingers; Gibson et al., 1988), the even-specific aromatic residue (Ar10) may be tyrosine, phenylalanine, or histidine (Figure 1). Nevertheless, the particular aromatic residue seen in an *individual* domain is invariant among vertebrates *in that domain* (Figure 1), suggesting a functional constraint in the evolutionary history of the gene. What structural similarities may account for the diversity of aromatic residues at the swapped site, and conversely, what differences may enjoin their invariance among individual domains?

The NMR structure of a tyrosine-containing domain has been determined (ZFY-6; Kochoyan et al, 1991a,b). To investigate the structural implications of variant aromatic residues at position 10, we have determined the 2D-NMR structures of the mutant domains Tyr10Phe (designated ZFY-*phe*) and Tyr10His (designated ZFY-*his*) (Figure 2A). These analogues retain the canonical $\beta\beta\alpha$ motif and in each case exhibit staggered-horizontal stacking between the variant aromatic residue and the proximal histidine (His21) in the hydrophobic core (Figure 6). ZFY-*phe* is essentially identical to ZFY-6 in overall structure, thermodynamic stability, and rates of amide–proton exchange in D_2O. A small shift is observed in the position of the Phe10 aromatic ring, which may be rationalized by the requirement to bury a nonpolar surface (the end of the phenylalanine ring) or expose a polar surface (the Tyr10 *p*-OH). The presence or absence of a side-chain hydrogen bond to Ser12-OH$_{\gamma}$ may also contribute this local change; analysis of the tyrosine-specific Fermi vibrational doublet by laser Raman spectroscopy demonstrates that Tyr10 *p*-OH is accepting a hydrogen bond, which would not be possible in the case of Phe10 (T. Li, M. A. Weiss, and G. J. Thomas, Jr., manuscript in preparation). Although the average structure of ZFY-*his* is also similar to that of the parent peptide, the mutant domain is less dynamically stable by a number of criteria, including amide–proton exchange rates and conformational averaging of coupling constants. The thermodynamic stability of ZFY-*his* (as monitored by pH-dependent unfolding) is also reduced. Decreased pH stability of a His10-containing analogue has previously been observed in ZFY domain 8 but could not be ascribed specifically to the presence of His10 due to multiple sequence differences in the peptide (Weiss et al., 1990).

In summary, comparative studies of native and mutant Zn fingers provide insight into mechanisms by which a simple sequence template encodes a characteristic structure and protein surface. The present study is motivated by patterns of sequence conservation and variation in a gene family and demonstrates how the stability of the Zn finger is regulated by the identity of the central aromatic residue. Tyrosine, phenylalanine, and histidine at the swapped site each exhibit staggered-horizontal aromatic packing (Burley & Petsko, 1988) in the hydrophobic core and alter the structure or dynamics of the putative DNA-binding surface. The present studies also provide a baseline for future studies of nonaromatic analogues (Weiss & Keutmann, 1990; Mortishire-Smith et al., 1992), such as leucine or cyclohexylalanine. Correlation of the properties of substituents (e.g., size, hydrophobicity, aromaticity) with the stability, structure, and dynamics of mutant domains may enable the chemical contributions to a "protein-folding code" to be dissected.

ACKNOWLEDGMENT

We thank H. T. Keutmann and C. E. Dahl for peptide synthesis and purification; M. Kochoyan and J. P. Lee for assistance with NMR measurements; D. A. Case and P. E. Wright for the coordinates of Xfin-31; N. Pavletich and C. O. Pabo for the coordinates of the Zif268–DNA complex; G. M. Clore and A. Gronenborn for the coordinates of an enhancer-binding finger; T. F. Havel for the program DGII and advice; A. T. Brunger and M. Nilges for XPLOR and advice; C. Redfield for *J*-coupling simulation software; S. K. Burley and G. A. Petsko for discussion of aromatic–aromatic interactions; A. Bax, D. J. Patel, G. Wagner, and P. E. Wright for advice regarding NMR methods; and M. Karplus, D. C. Page, P. A. Sharp, and C. T. Walsh for discussion and communication of results prior to publication. NMR spectra were obtained at the Harvard Medical School NMR Facility.

SUPPLEMENTARY MATERIAL AVAILABLE

Two tables giving DG/SA restraints and two figures showing Ramachandran plots and NMR spectra of ZFY analogues at

different temperatures (14 pages). Ordering information is given on any current masthead page.

REFERENCES

Akke, M., Drakenberg, T., & Chazin, W. J. (1992) *Biochemistry 31*, 1011–1020.

Berg, J. M. (1988) *Proc. Natl. Acad. Sci. U.S.A. 85*, 99–487.

Berg, J. M. (1990) *Annu. Rev. Biophys. Biophys. Chem. 19*, 405–421.

Bowie, J. U., Reidhaar-Olson, J., F., Lim, W. A., & Sauer, R. T. (1990) *Science 247*, 1306–1310.

Burley, S. K., & Petsko, G. A. (1985) *Science 229*, 23–28.

Burley, S. K., & Petsko, G. A. (1986) *J. Am. Chem. Soc. 108*, 7995.

Burley, S. K., & Petsko, G. A. (1988) *Adv. Protein Chem. 39*, 125–189.

Churchill, M. E. A., Tullius, D. T., & Klug, A. (1990) *Proc. Natl. Acad. Sci. U.S.A. 87*, 5528–5532.

DiLella, A. G., Page, D. C., & Smith, R. G. (1990) *New Biol. 2*, 49–55.

Fairall, L., Rhodes, D., & Klug, A. (1986) *J. Mol. Biol. 192*, 577–591.

Frankel, A. D., Berg, J. M., & Pabo, C. O. (1987) *Proc. Natl. Acad. Sci. U.S.A. 84*, 4841–4845.

Gibson, T. J., Postma, J. P. M., Brown, R. S., & Argos, P. (1988) *Protein Eng. 2*, 209–218.

Hoch, J. C., Dobson, C. M., & Karplus, M. (1982) *Biochemistry 21*, 132–140.

Jasanoff, A., Kochoyan, M., Fraenkel, E., Lee, J. P., & Weiss, M. A. (1992) *J. Mol. Biol. 225*, 1035–1047.

Johnson, C. E., & Bovey, F. A. (1958) *J. Chem. Phys. 29*, 1012–1017.

Karlstrom, G., Linse, P., Wallqvist, A., & Jonsson, B. (1983) *J. Am. Chem. Soc. 105*, 3776–3782.

Klevit, R. E. (1991) *Science 253*, 1367.

Klevit, R. E., Herriol, J. R., & Horvath, S. (1990) *Proteins 7*, 214–226.

Klug, A., & Rhodes, D. (1987) *Trends Biochem. Sci. 12*, 464–468.

Kochoyan, M., Havel, T. F., Nguyen, D., Dahl, C. E., Keutmann, H. T., & Weiss, M. A. (1991a) *Biochemistry 30*, 3371–3386.

Kochoyan, M., Keutmann, H. T., & Weiss, M. A. (1991b) *Biochemistry 30*, 7063–7072.

Kochoyan, M., Keutmann, H. T., & Weiss, M. A. (1991c) *Proc. Natl. Acad. Sci. U.S.A. 88*, 8455–8459.

Kochoyan, M., Keutmann, H. T., & Weiss, M. A. (1991d) *Biochemistry 30*, 9396–9402.

Lee, M. S., Gippert, G. P., Soman, K. V., Case, D. A., & Wright, P. E. (1989a) *Science 245*, 635–637.

Lee, M. S., Cavanagh, J., & Wright, P. E. (1989b) *FEBS Lett. 254*, 159–164.

Mortishire-Smith, R. J., Lee, M. S., Bolinger, L., & Wright, P. E. (1992) *FEBS Lett. 296*, 11–15.

Nardelli, J. Gibson, T. J., Vesque, C., & Charnay, P. (1991) *Nature 349*, 175–178.

Nietfeld, W., El-Baradi, T., Mentzel, H., Pieler, T., Koster, M., Omichinski, J. G., Clore, G. M., Apella, E., Sakaguchi, K., & Gronenborn, A. M. (1990) *Biochemistry 29*, 9324–9334.

Page, D. C., Mosher, R., Simpson, E., Fisher, E. M. C., Mardon, G., Pollack, J., McGillivray, B., de la Chapelle, A., & Brown, L. G. (1987) *Cell 51*, 1091–1104.

Palmer, A. G., III, Rance, M., & Wright, P. E. (1991) *J. Am. Chem. Soc. 113*, 4371–4380.

Pardi, A., Balleter, M., & Wuthrich, K. (1984) *J. Mol. Biol. 180*, 741.

Parraga, G., Horvath, S. J., Eisen, A., Taylor, W. E., Hood, L., Young, E. T., & Klevit, R. E. (1988) *Science 241*, 1489–1492.

Pavletich, N. P., & Pabo, C. O. (1991) *Science 252*, 809–817.

Redfield, C., & Dobson, C. M. (1990) *Biochemistry 29*, 7201.

Richardson, J. S., & Richardson, D. C. (1988) *Science 240*, 1648–1652.

Schneider-Gadicke, A., Beer-Romero, P., Brown, L. G., Nussbaum, R., & Page, D. C. (1989) *Cell 57*, 1247–1258.

Smith, L. J., Sutcliffe, M. J., Redfield, C., & Dobson, C. M. (1991) *Biochemistry 30*, 986–996.

Weiss, M. A., & Hoch, J. C. (1987) *J. Magn. Reson. 72*, 324–333.

Weiss, M. A., & Keutmann, H. T. (1990) *Biochemistry 29*, 9808–9813.

Weiss, M. A., Mason, K. A., Dahl, C. E., & Keutmann, H. T. (1990) *Biochemistry 29*, 5660–5664.

Wuthrich, K. (1986) *NMR of Proteins and Nucleic Acids*, Wiley, New York.